Image Fusion Using Gaussian Mixture Models

Katie Heaps[1]
heaps006@umn.edu
Josh Koslosky[1]
kosl0052@umn.edu
Glenn Sidle[2]
sidleg@duq.edu
Stacey Levine[2]
sel@mathcs.duq.edu

[1] Department of Mathematics
University of Minnesota
Minneapolis, MN, USA

[2] Department of Mathematics and
Computer Science
Duquesne University
Pittsburgh, PA, USA

Abstract

In recent years, a number of works have demonstrated that processing images using patch-based features provides more robust results than their pixel based counterparts. A contributing factor to their success is that image patches can be expressed sparsely in appropriately defined dictionaries, and these dictionaries can be tuned to a variety of applications. Yu, Sapiro and Mallat [24] demonstrated that estimating image patches from multivariate Gaussians is equivalent to finding sparse representations in a structured overcomplete PCA-based dictionary. Furthermore, their model reduces to a straightforward piecewise linear estimator (PLE). In this work we show how a similar PLE can be formulated to fuse images with various linear degradations and different levels of additive noise. Furthermore, the solution can be interpreted as a sparse patch-based representation in an appropriately defined PCA dictionary. The model can also be adapted to better preserve edges and increase PSNR by adapting the level of smoothing to each local patch.

1 Introduction

In recent years, a number of successful models have been developed for processing images using patch-based features (see e.g. [10] and references therein). Often critical to this approach is that natural image patches can be expressed sparsely in appropriately defined dictionaries which can be tuned to a variety of applications.

In this work we consider the following image degradation model. Suppose an image f has undergone some linear degradation U (e.g. linear blur, pixel loss, subsampling, etc.) and is corrupted by additive noise $w \sim \mathcal{N}(0,\sigma^2)$. Then the observed, degraded data can be written as $y = Uf + w$. The goal is to recover f from y. Decomposing f into overlapping $\sqrt{n} \times \sqrt{n}$ *vectorized* patches $f_i \in \mathbb{R}^n$ for $i = 1..,I$ and noting that each patch may have undergone a unique linear degradation U_i and contains different additive noise w_i we can express the degraded image patches as $y_i = U_i f_i + w_i$ for $i = 1,..,I$. Recovering f from y now becomes the problem of recovering f_i from y_i and rebuilding f from the clean patches $\{f_i\}_{i=1}^I$.

The sparse dictionary model for solving this problem can be formulated as follows [9]. Given a dictionary $D \in \mathbb{R}^{n\times k}$ where $n \leq k$ (D can either be fixed or learned from the data), for each degraded image patch, y_i, one wishes to find a sparse coefficient vector $\alpha_i \in \mathbb{R}^k$ such that $f_i \approx D\alpha_i$. The optimal coefficients are typically recovered by solving

$$\hat{\alpha}_i = \arg\min_{\alpha\in R^k} \lambda||\alpha||_p + \frac{1}{2}||U_i D\alpha - y_i||_2^2 \tag{1}$$

where $p = 0$ or 1 is most commonly used for inducing sparsity, and $\lambda > 0$ is fixed and determined by the noise level.

In [24], the authors proposed a technique for solving generalized inverse problems using a piecewise linear estimator (PLE) that selects the best patch approximation from a fixed number of multivariate Gaussians. The authors demonstrate this approach performs better than (1) as well as other state-of-the-art approaches for a number of linear degradations. Of particular note is that the coherence of the dictionary is no longer a problem for challenging applications such as deblurring and zooming.

In this work we propose a model for fusing multiple images, $y^1,...,y^J$ of the same field of view into a single image f with optimal properties from each one. Image fusion is used in a number of applications where a single image is desired from multi-channel data that retains desirable information from each channel. This is a problem in military and medical applications e.g [13, 15, 19], images with different depths of focus e.g. [12, 16, 21], panchromatic zooming of satellite images e.g. [2, 26], simultaneous image fusion with super-resolution [23], and fusing noisy image bursts [4], blurry image stacks [18], or noisy/blurry pairs e.g. [3, 25], an application of particular interest in photography. Due to space limitations, an exhaustive list of applications would be impossible to include here. But these are a few examples of the wide range of applications that a generic image fusion model may be able to address.

To this end, we propose a general framework for fusing a set of degraded images $y^1,...,y^J$ that may have different levels additive noise, $w^1,...,w^J$, as well as different linear degradations, $U^1,...,U^J$. We use a patch based approach given its robustness as well as flexibility. A simple extension of (1) would be to solve for image patches $f_i \approx D\hat{\alpha}_i$, where

$$\hat{\alpha}_i = \arg\min_{\alpha\in R^k} ||\alpha||_p + \sum_{j=1}^{J} \frac{1}{2\lambda^j}||U_i^j D\alpha - y_i^j||_2^2. \tag{2}$$

However, whether D is a fixed or learned dictionary, (2) has some inherent challenges. If $p = 0$, although this non-convex functional can be solved using a pursuit algorithm [21, 22], these pursuit algorithms generally require an *ordering* of the most influential dictionary elements for a given patch f. However, the most influential dictionary elements may vary across the multi-channel data, presenting some challenges. If $p = 1$, certain common linear degradation operators U (e.g. subsampling and convolution) do not guarantee the *Restrictive Isometry Property* [5, 8] which is typically used to guarantee sparsity when minimizing the l_1 norm. It is possible to construct dictionaries that can still handle these issues for a single degradation operator, but this becomes quite restrictive when trying to fuse images with different degradations.

We show that the general approach for solving inverse problems in [24] has a natural extension to the image fusion problem which avoids some of the above mentioned concerns. The first primary benefit is its ease in formulation and implementation. There are no parameters to be tweaked, and it has a simple closed form solution. The second benefit is that as

shown in [24], it outperforms comparable methods when applied to single image restoration, in particular, when restoring low resolution or blurry images. Finally, it naturally lends itself to simple modifications that can assist in e.g. edge enhancement by weighting a single region differently across multiple images, depending on the level of detail and degradation in the given channel.

The rest of the paper is organized as follows. In section 2 we describe the model and its implementation. In section 3 we describe how solving the GMM based fusion model is equivalent to solving a sparse dictionary representation problem. Results are contained in section 4.

2 The Basic Image Fusion Model

2.1 Background

Yu Sapiro and Mallat [24] proposed a simple yet powerful algorithm for solving the following general inverse problem: recover a 'true image' f from a degraded image $y = Uf + w$ where U is a linear operator and w is additive Gaussian noise. The linear degradation U can be the identity operator (in the case of denoising) or may represent common degradations such as pixel loss (masking), blurring, or subsampling. This problem can be particularly challenging when using a dictionary based approach since the coherence of the dictionary with respect to the degradation operator U plays a critical role in successful signal recovery. The authors in [24] proposed a probabilistic based approach using Gaussian Mixture Models aimed to solve inverse problems with a variety of degradation operators, U, which they demonstrate is comparable to or improves upon state of the art techniques.

The degraded image, y, is decomposed into vectorized $\sqrt{n} \times \sqrt{n}$ blocks, $y_i = U_i f_i + w_i$, for $i = 1, ..., I$. The idea is that these image patches can be described by a mixture of multivariate Gaussian distributions with appropriately defined means and covariance matrices. Assuming we are given K multivariate Gaussians $\{\mathcal{N}(\mu_k, \Sigma_k)\}_{1 \le k \le K}$ parametrized by their means $\mu_k \in \mathbb{R}^n$ and covariance matrices $\Sigma_k \in \mathbb{R}^{n \times n}$, each reconstructed patch f_i is drawn from one of these Gaussians (which are equally likely) for some $k_i \in \{i, ..., K\}$ according to the probability density function

$$p(f_i) = \frac{1}{(2\pi)^{N/2} |\Sigma_{k_i}|^{1/2}} \exp\left(-\frac{1}{2} (f_i - \mu_{k_i})^T \Sigma_{k_i}^{-1} (f_i - \mu_{k_i}) \right). \tag{3}$$

Finding the optimal image patches becomes a non-convex optimization problem, but the authors in [24] proposed a maximum *a posteriori* expectation-maximization algorithm (MAP-EM) for solving this problem.

In this work, we demonstrate how this approach can be used to solve the image fusion problem in which any given number of images of the same field of view can be fused into a single image, retaining optimal properties from each one. We are not aware of other algorithms that easily adapt to the general fusion problem when variable linear degradations are involved. To this end, we assume we are given J degraded images of the same field of view,

$$y^1 = U^1 f + w^1, \ ..., \ y^J = U^J f + w^J.$$

For simplicity we assume the images are perfectly aligned, although the operators $U^1, ..., U^J$ may be different. Perfect alignment is a strong assumption, but our intent to propose a general framework. We thus refer the reader to a number of existing image registration algorithms (e.g. [1, 6, 14, 17]) that can be used for specialized applications.

2.2 MAP-EM Algorithm

2.2.1 Signal Estimation and Model Selection (E-step)

We assume that the number of Gaussians, K and their parameters $\{(\mu_k, \Sigma_k)\}_{1\le k\le K}$ are known (we discuss the initialization in section 2.3) and estimate the signal patches by maximizing the log *a-posteriori* probability, $\log p(f_i|y_i^1,...,y_i^J,\Sigma_k)$ for each k, as given in (3). We assume that $f_i \sim \mathcal{N}(0,\hat{\Sigma}_k)$ and $w_i^j \sim \mathcal{N}(0,\sigma_j^2 Id)$ for $j = 1,...,J$ where Id is the identity matrix. For each patch $i = 1,...,I$, we wish to maximize the following log a-posteriori likelihood, which using Bayes rule is

$$\begin{aligned}(\hat{f}_i,\hat{k}_i) &= \arg\max_{f,k} \log p(f|y_i^1,...,y_i^J,\hat{\Sigma}_k)\\ &= \arg\max_{f,k} \sum_{j=1}^{J} \log p(y_i^j|f_i,\hat{\Sigma}_k) + \log p(f_i|\hat{\Sigma}_k)\\ &= \arg\min_{f,k} \sum_{j=1}^{J} \left(\frac{1}{\sigma_j^2}||U_i f - y_i^j||^2\right) + f^T\hat{\Sigma}_k^{-1} f + \log|\hat{\Sigma}_k| \end{aligned} \tag{4}$$

For each fixed k in (4), a simple linear filter gives the minimizer with respect to f as

$$f_i^k = \sum_{j=1}^{J} W_{k,i}^j y_i^j \quad \text{where} \quad W_{k,i}^j = \hat{\Sigma}_k \left(\sum_{l=1}^{J} \frac{1}{\sigma_l^2}(U_i^l)^T U_i^l \hat{\Sigma}_k + Id\right)^{-1} (U_i^j)^T. \tag{5}$$

Then for $i = 1,...,I$, the solution of (4) is given by the pair

$$\hat{f}_i = f_i^{\hat{k}_i} \quad \text{where} \quad \hat{k}_i = \arg\min_{k\in\{1,...,K\}} \sum_{j=1}^{J} \left(\frac{1}{\sigma_j^2}||U_i f_i^k - y_i^j||^2\right) + (f_i^k)^T\hat{\Sigma}_k^{-1} f_i^k + \log|\hat{\Sigma}_k|. \tag{6}$$

In practice K is small (we use $K = 19$), so $\hat{k}_i$ in (6) is found by simply calculating the energy for each $k = 1,...,K$ and finding the argument that yields the smallest value. Although each patch is estimated from a single Gaussian, the patches are overlapping (patches centered at every pixel in the image are used) and the overlapping patches are averaged at each location to produce the final result, so each pixel will typically contain a mixture of Gaussians.

2.2.2 Gaussian Model Parameter Estimation (M-Step)

Once the model selection $\hat{k}_i$ and signal estimation $\hat{f}_i$ are known for each patch, setting $C_k = \{i|\hat{k}_i = k\}$ for $k = 1,...,K$, the new Gaussian parameters are computed by

$$\hat{\mu}_k = \frac{1}{|C_k|}\sum_{i\in C_k} \hat{f}_i \quad \text{and} \quad \hat{\Sigma}_k = \frac{1}{|C_k|}\sum_{i\in C_k} (\hat{f}_i - \hat{\mu}_k)^T(\hat{f}_i - \hat{\mu}_k) \tag{7}$$

which satisfy $(\hat{\mu}_k,\hat{\Sigma}_k) = \arg\max_{\mu_k,\Sigma_k} p(\{\hat{f}_i\}_{i\in C_k}|\mu_k,\Sigma_k)$.

2.3 Initialization

The initialization of the Gaussian parameters μ_k and Σ_k are critical to the success of the model. We follow the initialization in [24] which is based on the observation that in many learned dictionaries, the dominant patches looked like edge elements of a fixed orientation.

Initialization:

1. Eighteen binary straight edge images of fixed orientations at 10^o increments from 0^o to 170^o were generated.
2. For each of the 18 edge images,
   (a) the edge image is randomly sampled until a nonsingular covariance matrix can be formed from the data.
   (b) the dominant eigenvector of the covariance matrix (which is almost DC) is set to be a constant and Gram-Schmidt is used to guarantee the PCA basis is orthonormal. Then for $k = 1,...,18$, $\Sigma_k = B_k \Lambda_k B_k^t$, where $B_k = [b_k^1 \dots b_k^n]$ is the orthonormal PCA basis and $\Lambda_k = diag(\lambda_k^1,...,\lambda_k^n)$ is the diagonal matrix of associated (decreasing) eigenvalues. For simplicity, $\mu_k = 0$.
3. A 19^{th} Gaussian was created based on the Discrete Cosine Transform to allow for more variability in the textures, yielding $K = 19$ total Gaussians.
4. If the fusion involves a blurring operator for *any* y^j, $j = 1,...,J$, a hierarchical basis is used incorporating a second layer of varying positions for each of the directional PCA bases described above. We refer the reader to [24] Section VII.A for more details.

Remark: An alternate initialization derived from natural images was recently proposed [20] for a SURE (Stein's Unbiased Risk Estimator) guided Piecewise Linear Estimator (S-PLE). The model in [20] is intended for denoising, for which it is both quite successful and mathematically well motivated. To the best of our knowledge, it has not yet been extended to image data that has undergone linear degradations, but this opens up a new line of research in the consideration of alternate initializations, particularly for specialized applications.

3 Sparse Patch-Based Modeling

The MAP-EM algorithm described in section 2.2 has a direct sparse modeling interpretation. A straightforward computation shows that the solution in (5) is precisely $f_i^k = B_{k_i} a_i^k$ where

$$a_i^k = \arg\min_{a \in \mathbb{R}^n} \left(\sum_{j=1}^{J} \frac{1}{\sigma_j^2} ||U_i^j B_k a - y_i^j||^2 + \sum_{m=1}^{N} \frac{|a[m]|^2}{\lambda_m^k} \right). \tag{8}$$

Here B_k is the orthonormal PCA basis diagonalizing the covariance matrix Σ_k and the λ_m^k are the corresponding eigenvalues in decreasing order. Although the second term in (8) is a weighted l_2 norm, it favors dominant eigenvectors and the eigenvalues rapidly decrease in magnitude [24], thus inducing sparsity. Furthermore, the PCA basis B_k and the eigenvalues incorporate information from the data in the *M-Step*, so this model promotes collaborative filtering in which the dictionary is learned from the data.

Dictionary construction is particularly important when allowing for linear degradations U_i since here we assume $y_i = U_i B_k a_i + w_i$, and while each of the dictionaries B_k might satisfy 'good' dictionary properties (e.g. sparsity, recoverability, and stability [24]), $U_i B_k$ might not. For example, if B_k contained the atoms $b_1 = (1,1,1,...1)^T$ and $b_2 = (1,-1,1,-1,...,-1)^T$ and U_i were a subsampling operator, then $U_i b_1 = (1,1,1,...1)^T = U_i b_2$ and stability would be violated. In this case it is equally likely that a sparsity inducing model such as (1) would choose b_2 as b_1 to best represent a smooth region, which could be disastrous for the final result. The initialization and parameter estimation described in section 2 avoid this problem.

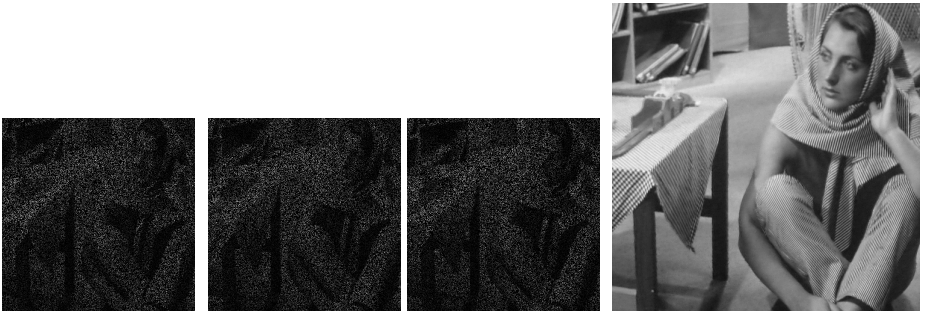

(a) (b) (c) (d)

Figure 1: (a), (b), (c): images of the same field of view with random 80% masking, (d): the final fused result using the proposed approach.

Figure 2: Left: Result of running the single image MAP-EM algorithm on the masked image from figure 1(a) only, PSNR = 26.1547; Middle: Result of running the single image MAP-EM algorithm on the average of the masked images in figure 1, PSNR = 30.8393; Right: Result of the proposed fusion model (close up the result in figure 1), PSNR = 32.5033.

4 Results

We tested the fusion model on several sets of images involving varying noise levels and linear degradations. Our patch sizes are all 8×8, so $n = 64$. In [24] the authors provide a number of examples that confirm that except in the case of denoising (where BM3D [7] still seems to outperform all comparable models), the single image PLE using the MAP-EM algorithm generally provided state-of-the art results for difficult problems involving linear degradations, inlcuding deblurring and subsampling. Given the range of applied fusion problems, we provide here several examples to demonstrate the ease and success of the model for fusing image sets with a variety of degradations. Our intent is to provide a proof of concept, opening the door to more specialized applications by the user. For simplicity we assume the images are perfectly aligned, although many real world problems do not afford this luxury. In the latter case, one could choose to preprocess the data with an existing image warping algorithm, e.g. [1, 6, 14, 17].

Figure 1 contains a set of images with varying degrees of masking and the final fused

Table 1: PSNR: PLE [24] -vs- PLE with adaptive smoothing (9)-(10); tests performed on the standard image database with noise level σ=25; the average increase in PSNR is 0.42.

Image	noisy image	GMM [24]	GMM+AS (9)-(10)
Barbara	20.1721	27.6023	28.0768
Blonde	20.1664	28.9708	29.2502
Boat	20.201	25.277	26.1944
Bridge	20.1607	25.1989	25.6419
Brunette	20.1696	33.78	33.8809
Cameraman	20.1783	31.4219	31.5926
Fair	20.1702	28.3473	28.6918
Lena	20.1711	30.8052	31.0635
Oldies	20.1787	28.244	28.5609
Peppers	20.1347	27.515	28.1031
Plane	20.1806	29.4183	30.1749

result using the proposed model. In figure 2, we compare the result of recovering the image from a single masked image using the model in [24], the result of simply averaging the 'known pixels' from the masked images in figures 1(a-c) and running the single image piecewise linear estimator from [24], and the result using the fusion model proposed here. We note both the increase in PSNR, as well as visual improvements which include smoother homogeneous regions while preserving edges and textures.

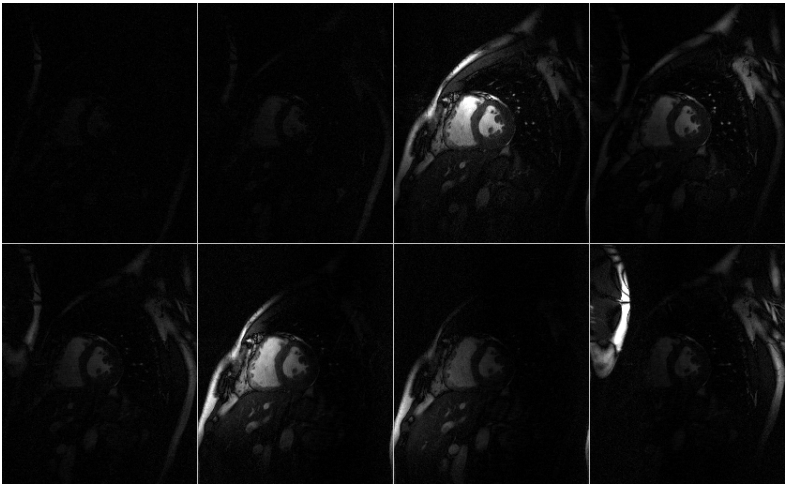

Figure 3: 8 coil MRI image, data courtesy of Mark Griswold.

We also modified the denoising model to be able to handle both spatially variable noise levels as well as treat smooth and textured/edge regions differently. This was incorporated into the model by making the noise level σ vary depending on the characteristics of each patch i. In this case we wish to solve

$$\min_{f,k} \sum_{j=1}^{J} \left(\frac{1}{\sigma_{ij}^2} ||U_i f - y_i^j||^2 \right) + f^T \hat{\Sigma}_k^{-1} f + \log|\hat{\Sigma}_k| \tag{9}$$

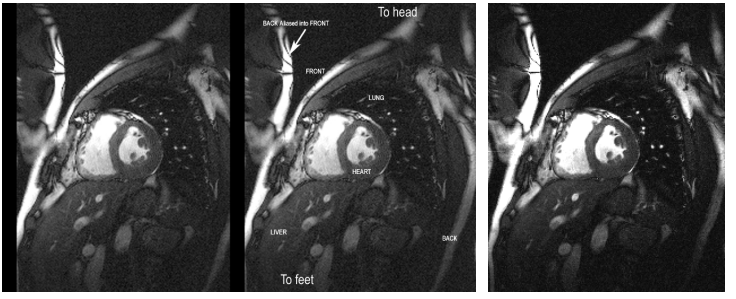

(a) (b)

Figure 4: Results of fusing the 8 coils in figure 3: (a) Result from [11], (b) Result from the proposed method.

where σ_{ij} is either the estimated noise level in image j at patch i, or is weighted depending on edge information, such as

$$\sigma_{ij} = \sigma_j \times \left(\frac{1}{1 + k|\nabla G_\tau * y_i|^2} + 0.5 \right). \tag{10}$$

Here σ_j is the estimated noise level for the entire image, G_τ is a Gaussian of standard deviation τ and $k > 0$ is a positive parameter. Note that in patches containing high gradient information (likely edges), $|\nabla G_\tau * y_i|$ will be large so the so the local noise level $\sigma_{ij} \approx \frac{\sigma_j}{2}$, yielding less smoothing. In patches with low variations in the gradient, likely smooth regions, the local noise level $\sigma_{ij} \approx \frac{3\sigma_j}{2}$. In our experiments we set $\tau = .07$ (for a noise level of $\sigma_j = 25$) and $k = 0.0075$ (for images with intensity in the range [0,255]). These parameters can be locally optimized, but we found this worked fairly well in getting a general improvement on the standard image database (see table 1). It is important to point out that this model does not necessarily give state of the art results with respect to denoising alone (for example, BM3D [7] consistantly achieves better results). The power in the proposed model is the general framework in which images with multiple degradations can be combined.

We also tested the proposed fusion model on an 8 coil parallel MRI image dataset. The final fused result should retain fine features (e.g. vessels in the lung) while not introducing spurious features. Typical variational denoising methods can lead to the oversmoothing of fine features for this kind of data, and the more detail preserving techniques often lead to staircasing and thus unwanted artifacts. The noise level is uniform throughout a single coil, but varies between coils. A simple application of our fusion model preserved fine detail while attenuating noise.

Our final example is the fusion of a noisy-blurry pair, an application that could arise when images with varying exposure times are combined into a single image. Noisy and blurry versions of the color image in figure 5 were processed separately as well as fused using the proposed model to obtain a result that incorporated information from both images in the set (color channels were processed separately). The intensity cross sections in figure 6 were typical for flat and detailed regions in the image, and demonstrate how the model readily extracts the relevant information from the images being fused; the flat regions are closer to the original color than denoising alone, and the details are more accurately preserved than deblurring alone. Figure 7 contains a close up view of a grassy region below the plane to

(a) (b) (c)

(d) (e) (f)

Figure 5: First row: (a) blurry image, PSNR=27.5454 (b) noisy image, PSNR=29.2852, (c) original clean image; Bottom row: (d) deblurred image only, PSNR=31.3776, (e) denoised image only, PSNR=33.4498, (f) result of fusing the noisy/blurry pair; that is, both images from the first row, PSNR=35.7534.)

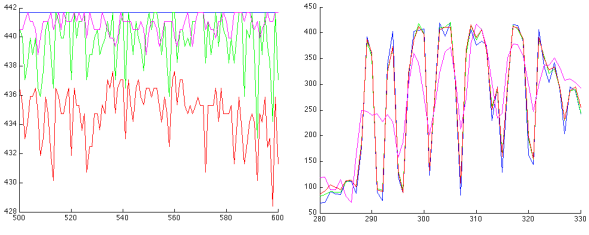

(a) (b)

Figure 6: *Typical cross-sections of the magnitude of the intensity*: (a) flat region of the sky (b): detailed region across the lettering on the plane (blue=original image, green=fused result, red=denoised only, magenta=deblurred only).

(a) (b) (c) (d)

Figure 7: *Close up of a typical textured region*: (a) result of deblurring the image in figure 5(a); (b) result of denoising the image in figure 5(b); (c) result of the proposed fusion model; (d) the original clean image

illustrate the level of detail preserved in the textured regions of the fused image.

We should note that a number of successful models exist for specialized problems in image fusion. Our intent is to propose a simple, flexible, and general framework for fusing images containing noise and linear degradations, and illustrate the behavior and potential of fusing images in this framework.

Acknowledgements

We would like to thank Guoshen Yu, Guillermo Sapiro and John Kern for their helpful discussions. The last author was funded in part by NSF-DMS #0915219.

References

[1] http://www.revisionfx.com/products/twixtor/.

[2] Coloma Ballester, Vicent Caselles, Laura Igual, Joan Verdera, and Bernard Rougé. A variational model for p+xs image fusion. *International Journal of Computer Vision*, 69 (1):43–58, 2006.

[3] M. Bertalmio and S. Levine. Variational approach for the fusion of exposure bracketed pairs. *Image Processing, IEEE Transactions on*, 22(2):712–723, 2013. ISSN 1057-7149.

[4] A. Buades, Y. Lou, J. M. Morel, and Z. Tang. A note on multi-image denoising. *Proceedings of the International Workshop on Local and Non-Local Approximation (LNLA) in Image Processing*, August 2009.

[5] E.J. Candes, J. Romberg, and T. Tao. Robust uncertainty principles: exact signal reconstruction from highly incomplete frequency information. *Information Theory, IEEE Transactions on*, 52(2):489–509, 2006.

[6] I.J. Cox, S.L. Hingorani, S.B. Rao, and B.M. Maggs. A maximum likelihood stereo algorithm. *Computer vision and image understanding*, 63(3):542–567, 1996.

[7] K. Dabov, A. Foi, V. Katkovnik, and K. Egiazarian. Image denoising by sparse 3-d transform-domain collaborative filtering. *Image Processing, IEEE Transactions on*, 16 (8):2080–2095, 2007.

[8] D.L. Donoho. Compressed sensing. *Information Theory, IEEE Transactions on*, 52(4): 1289–1306, 2006.

[9] M. Elad, M.A.T. Figueiredo, and Yi Ma. On the role of sparse and redundant representations in image processing. *Proceedings of the IEEE*, 98(6):972 –982, June 2010.

[10] Michael Elad. Sparse and redundant representation modeling - what next? *Signal Processing Letters, IEEE*, 12(12):922 – 928, 2012.

[11] M. Griswold, D. Walsh, R. Heidemann, A. Haase, and P. Jakob. The Use of an Adaptive Reconstruction for Array Coil Sensitivity Mapping and Intensity Normalization. In *Proc. Intl. Soc. Mag. Reson. Med.*, volume 10. ISMRM, 2002.

[12] Shutao Li, James T. Kwok, and Yaonan Wang. Multifocus image fusion using artificial neural networks. *Pattern Recogn. Lett.*, 23(8):985–997, June 2002.

[13] N. Mitianoudis and T. Stathaki. Adaptive image fusion using ica bases. In *Acoustics, Speech and Signal Processing, 2006. ICASSP 2006 Proceedings. 2006 IEEE International Conference on*, volume 2, pages II–II, 2006.

[14] N. Papenberg, A. Bruhn, T. Brox, S. Didas, and J. Weickert. Highly accurate optic flow computation with theoretically justified warping. *International Journal of Computer Vision*, 67(2):141–158, 2006.

[15] Xiao-Bo Qu, Guo-Fu Xie, Jing-Wen Yan, Zi-Qian Zhu, and Ben-Gang Chen. Image fusion algorithm based on neighbors and cousins information in nonsubsampled contourlet transform domain. In *Wavelet Analysis and Pattern Recognition, 2007. ICWAPR '07. International Conference on*, volume 4, pages 1797–1802, 2007.

[16] R. Redondo, F. Šroubek, S. Fischer, and G. Cristóbal. Multifocus image fusion using the log-gabor transform and a multisize windows technique. *Inf. Fusion*, 10(2):163–171, April 2009.

[17] Y. Shinagawa and T.L. Kunii. Unconstrained automatic image matching using multiresolutional critical-point filters. *IEEE Transactions on Pattern Analysis and Machine Intelligence*, pages 994–1010, 1998.

[18] F. Sroubek and J. Flusser. Multichannel Blind Deconvolution of Spatially Misaligned Images. *IEEE Transactions on Image Processing*, 14(7):874–883, 2005.

[19] Tao Wan, N. Canagarajah, and A. Achim. Compressive image fusion. In *Image Processing, 2008. ICIP 2008. 15th IEEE International Conference on*, pages 1308–1311, 2008.

[20] Y.-Q. Wang and J.M. Morel. Sure guided gaussian mixture image denoising. *HAL: hal-00785334, version 1*, 2013.

[21] Bin Yang and Shutao Li. Multifocus image fusion and restoration with sparse representation. *Instrumentation and Measurement, IEEE Transactions on*, 59(4):884–892, 2010.

[22] Bin Yang and Shutao Li. Pixel-level image fusion with simultaneous orthogonal matching pursuit. *Inf. Fusion*, 13(1):10–19, January 2012.

[23] Haitao Yin, Shutao Li, and Leyuan Fang. Simultaneous image fusion and super-resolution using sparse representation. *Information Fusion*, 14(3):229 – 240, 2013.

[24] Guoshen Yu, Guillermo Sapiro, and Stephan Mallat. Solving inverse problems with piecewise linear estimators: From gaussian mixture models to structured sparsity. *IEEE Trans. Image Process.*, 21(5):2481– 2499, 2012.

[25] Lu Yuan, Jian Sun, Long Quan, and Heung-Yeung Shum. Image deblurring with blurred/noisy image pairs. *IACM Transactions on Graphics*, 26(3):1–10, 2007.

[26] Sheng Zheng, Wen zhong Shi, Jian Liu, and Jinwen Tian. Remote sensing image fusion using multiscale mapped ls-svm. *Geoscience and Remote Sensing, IEEE Transactions on*, 46(5):1313–1322, 2008.